JACS
JOURNAL OF THE AMERICAN CHEMICAL SOCIETY

Article

pubs.acs.org/JACS

Quorum Activation at a Distance: Spatiotemporal Patterns of Gene Regulation from Diffusion of an Autoinducer Signal

Gabriel E. Dilanji,[†] Jessica B. Langebrake,[‡] Patrick De Leenheer,[‡] and Stephen J. Hagen*[,†]

[†]Department of Physics, University of Florida, Gainesville, Florida 32611-8440, United States

[‡]Department of Mathematics, University of Florida, Gainesville, Florida 32611-8105, United States

Supporting Information

ABSTRACT: Quorum sensing (QS) bacteria regulate gene expression collectively by exchanging diffusible signal molecules known as autoinducers. Although QS is often studied in well-stirred laboratory cultures, QS bacteria colonize many physically and chemically heterogeneous environments where signal molecules are transported primarily by diffusion. This raises questions of the effective distance range of QS and the degree to which colony behavior can be synchronized over such distances. We have combined experiments and modeling to investigate the spatiotemporal patterns of gene expression that develop in response to a diffusing autoinducer signal. We embedded a QS strain in a narrow agar lane and introduced exogenous autoinducer at one terminus of the lane. We then measured the expression of a QS reporter as a function of space and time as the autoinducer diffused along the lane. The diffusing signal readily activates the reporter over distances of ∼1 cm on time scales of ∼10 h. However, the patterns of activation are qualitatively unlike the familiar spreading patterns of simple diffusion, as the kinetics of response are surprisingly insensitive to the distance the signal has traveled. We were able to reproduce these patterns with a mathematical model that combines simple diffusion of the signal with logistic growth of the bacteria and cooperative activation of the reporter. In a wild-type QS strain, we also observed the propagation of a unique spatiotemporal excitation. Our results show that a chemical signal transported only by diffusion can be remarkably effective in synchronizing gene expression over macroscopic distances.

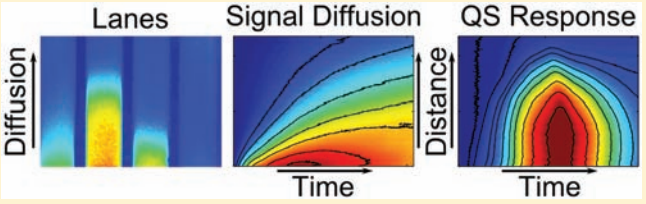

INTRODUCTION

Quorum sensing (QS) is a mechanism of bacterial gene regulation that is based on the synthesis and release of diffusible chemical signals known as autoinducers. At sufficiently high bacterial population densities, these autoinducers accumulate in the local environment and trigger population-wide changes in gene expression. QS plays a central role in the regulation of a variety of bacterial phenotypes, including biofilm formation, genetic competence, symbiosis, motility, and the production of virulence factors.[1−3] QS was originally interpreted simply as a means for bacteria within chemically and physically homogeneous cultures to assess their own population density, but it is now recognized as a complex behavior that facilitates microbial competition and cooperation in mixed-species colonies, coordinates symbiotic interactions and colonization, and may even allow a bacterium to characterize physical and chemical properties of its local environment.[4−6]

QS often occurs in environments that are physically, biologically, and chemically heterogeneous, such as biofilms and the rhizosphere. Here convection and mixing are inefficient, and chemical signals are transported primarily by diffusion.[7] Their stability and diffusive mobility must determine the distances and time scales over which they can activate gene expression. The widespread use of QS by diverse bacterial species therefore invites questions about the role of diffusion in QS regulation: one may ask how far and how fast an autoinducer signal can travel, how accurately its diffusion can coordinate gene expression in spatially extended colonies, and what type of spatial and temporal dynamics may occur when production of the autoinducer is subject to positive feedback. Since bacterial growth and diffusion of a signal through a colony proceed on similar time scales (minutes to hours), we expect that spatially and temporally heterogeneous patterns of gene expression should develop as QS signals diffuse across a spatially extended population. We also anticipate that the nonlinearities inherent in gene regulatory processes such as signal−receptor binding, promoter activation, and autofeedback in autoinducer production should cause spatiotemporal patterns of quorum-regulated gene expression to differ qualitatively from the patterns of spreading concentration that are generated by the diffusion equation alone.

Because QS research has traditionally focused on well-stirred systems, few experimenters have explored the spatial and temporal patterns of gene expression that result from diffusing quorum signals. Nevertheless, some authors have investigated the spatial range of quorum signaling and reported intriguing results for the diffusion of acyl homoserine lactone (AHL) autoinducers, which are widely used by Gram-negative proteobacteria. Gantner et al.[8] measured the physical distance between an autoinducer-sensing cell and the nearest autoinducer-synthesizing cell in fluorescent reporting strains of *Pseudomonas*

Received: December 12, 2011
Published: February 28, 2012

   dx.doi.org/10.1021/ja211593q | *J. Am. Chem. Soc.* 2012, 134, 5618−5626

putida. They found a wide distribution of such "calling distances" ranging from 5 μm to as much as 78 μm. More recently, Flickinger et al.[9] studied the interaction of populations via AHL diffusion in a *Pseudomonas aeruginosa* biofilm and found that quorum-regulated genes could be induced at distances as great as 8 mm from an AHL-producing strain. Whitaker et al.[10] used a fiber-optic array to study single-cell QS gene regulation using an autoinducer-sensing strain and found that temporal patterns of reporter gene expression are affected by both the cell density and the spatial configuration of the cells. Danino et al.[11] designed a synthetic QS-based oscillator circuit in which a diffusing AHL signal can trigger a wave of gene expression that travels hundreds of micrometers through a population of similarly engineered cells.

Such studies raise the question of whether we can construct quantitative models for the patterns of quorum-regulated gene expression arising from autoinducer diffusion through a bacterial colony. Here we imaged these spatial and temporal patterns (using a bioluminescence or *gfp* reporter) as they formed on macroscopic length scales (mm to cm) in bacterial cultures containing QS circuits based on the LuxI/LuxR system of *Vibrio fischeri* (see Figure 1). The bacteria were confined to narrow, effectively one-dimensional agar lanes to make the signal diffusion amenable to a precise mathematical description. An AHL signal introduced at one terminus of the lane spreads according to a one-dimensional diffusion equation,[12] activating the QS response as it travels. We modeled the reporter expression with a system of chemical kinetic equations that describes the bacterial response to the diffusing AHL[13,14] and compared the results from the model and the experiments.

We demonstrated this approach in a quorum "sensor" strain that cannot synthesize AHL but responds to exogenous AHL by expressing a *gfp* reporter. We found that diffusing AHL can generate patterns of gene expression that extend over distances of many millimeters and time scales of hours. These patterns are qualitatively unlike the simpler patterns formed by diffusion of, for example, a soluble dye. In fact, they show a surprising synchrony of gene expression over macroscopic distances, despite the inefficiency of diffusive transport. We also verified that similar patterns appear in the QS-regulated bioluminescence of a *V. fischeri* strain that lacks AHL-synthesis ability. Finally, we investigated the more complex case of a wild-type *V. fischeri* (strain MJ11) that synthesizes its own autoinducer. We found that its QS-regulated bioluminescence can exhibit a unique, wavelike excitation that propagates rapidly over macroscopic distances.

METHODS

Bacterial Cultures. Figure 1 shows the QS bacterial strains used in this work. The quorum "sensor" strain is *Escherichia coli* MT102 harboring plasmid pJBA132, which was constructed by Andersen et al[15] and contains the sequence *luxR*-P_{luxI}-*gfp*(ASV). The *gfp*(ASV) encodes a variant of green fluorescent protein (GFP) with a short half-life ($\leq$1 h), which prevents GFP from accumulating indefinitely during the measurements. This gives us greater sensitivity in tracking the bacterial response kinetics as AHL diffuses through the environment. The strain was provided by Dr. Fatma Kaplan.

Cultures in exponential phase were prepared by growing the *E. coli* to OD_{600} = 0.3 in Luria–Bertani (LB) medium, approximately pH 7, at 37 °C. The culture was prewarmed for 15 s at 50 °C to promote survival in warm agar[16] and then diluted 100× into molten 0.75% LB agar at 50 °C. Agar mix (250 μL) was then quickly pipetted into each of the four parallel lanes of a frame that is described below. The frame was sandwiched between two glass coverslips as the agar cooled. The

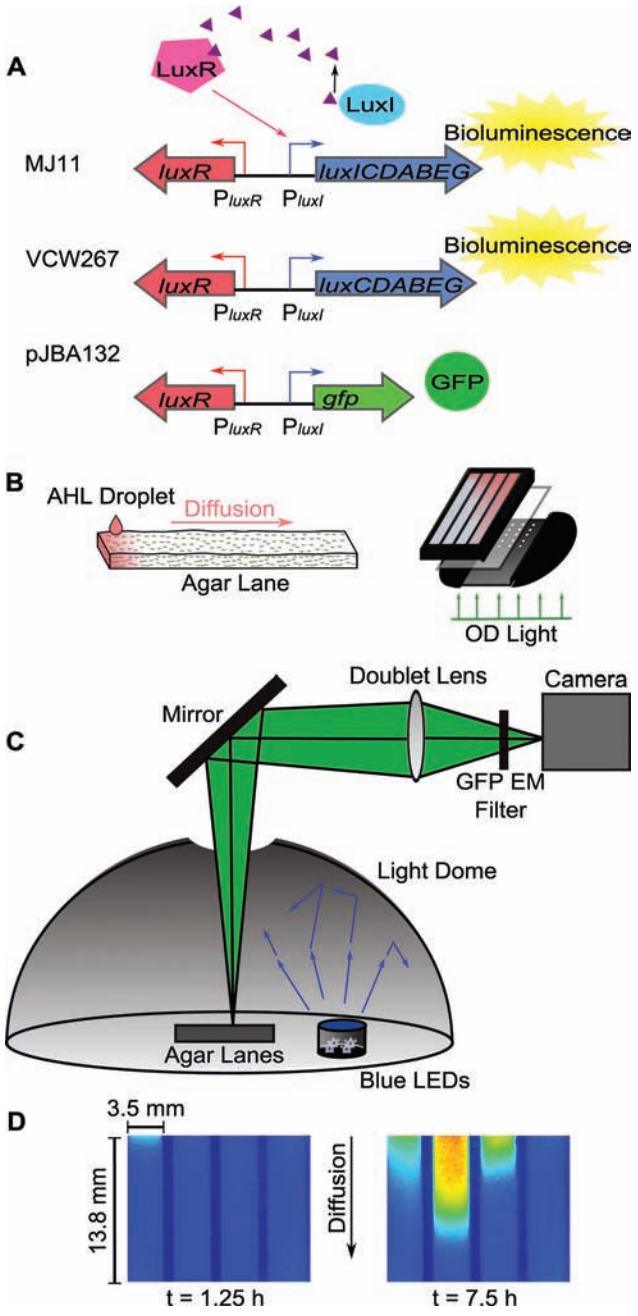

Figure 1. Experimental configuration: (A) Strains used in this study. MJ11 is a wild-type *V. fischeri* with an intact *lux* operon for synthesis (via LuxI) and detection (via LuxR) of the natural AHL signal (3OC6-HSL) and production of bioluminescence. VCW267 is a mutant *V. fischeri* lacking the AHL synthase (LuxI). The pJBA132 "sensor" strain of *E. coli* has a *gfp* reporter under control of the *luxI* promoter but lacks *luxI*. (B) (left) A droplet of autoinducer (3OC6-HSL) is deposited at one terminus of a rectangular block of agar in which live bacteria are uniformly embedded. The autoinducer diffuses down the lane, generating a pattern of QS activation in the bacteria. (right) Four independent bacteria/agar lanes are contained in a single frame that is supported by a glass coverslip and mounted under the light dome. (C) The light dome provides highly uniform, diffuse excitation light for imaging the GFP fluorescence of the bacteria in the lanes. The same optical configuration allows us to measure the bioluminescence and optical density of the samples in situ. (D) Representative fluorescence images (in false color) from a typical experiment with *E. coli* + pJBA132. Further details are provided in movies S1–S3 in the SI.

dx.doi.org/10.1021/ja211593q | *J. Am. Chem. Soc.* 2012, 134, 5618–5626

upper glass coverslip was then carefully removed, leaving a very flat and uniform slab of agar within each lane. The device was incubated at room temperature for 1.5 h before measurements began.

V. fischeri strain MJ11 is a wild-type strain that was derived from its symbiotic host fish *Monocentris japonicus* and provided to us by Dr. Mark Mandel. *V. fischeri* strain VCW267 is a synthase-deficient (−*luxI*) mutant produced from an ES114 wild-type background and was provided to us by Dr. Eric Stabb. Both strains were grown to OD_{600} = 0.3 in commercial photobacterium medium (no. 786230, Carolina Biological), approximately pH 6.9, at room temperature and then prepared as above for the agar lanes. The photobacterium medium is a rich medium composed of yeast extract, tryptone, phosphate buffer, and glycerol in artificial seawater.

Well-Plate Measurements. To obtain parameters for our mathematical model for *E. coli* + pJBA132 growth and its response to the AHL, we measured the optical density (OD) and fluorescence of this strain in the presence of AHL concentrations ranging from 0 to 500 nM. These data were collected in a multiwell plate using an automated plate reader (Biotek Synergy 2). An exponential phase culture (OD_{600} = 0.3) was diluted 100× into LB medium containing 0.1% agar. This inoculated medium was then loaded into individual wells containing *N*-(3-oxohexanoyl)-L-homoserine lactone [3OC6-HSL, CAS no. 143537-62-6, Sigma Chemical], which is the natural AHL of the LuxI/LuxR system. The GFP fluorescence and OD of each well were measured over a period of ∼25 h at room temperature. As described in the Supporting Information (SI), we then fit the resulting multidimensional data set (OD and GFP fluorescence × [AHL] × time) to the model summarized in Mathematical Model.

Lanes, Illumination, and Imaging. We recorded spatiotemporal patterns of QS regulation in bacteria/agar mixtures that were confined to rectangular lanes of length L = 32 mm and cross section 3.5 mm × 2 mm ($w \times d$). The lanes were designed with a small cross section relative to their length to ensure that diffusional equilibration across the transverse dimensions would proceed much faster (∼150×) than diffusion along the length L. Therefore, when AHL was deposited at a lane terminus, its concentration after ∼2 h could be considered uniform across the transverse dimension while showing a one-dimensional diffusion profile along the x (length) axis. (The one-dimensional character of diffusion in the lanes was verified by the dye diffusion study described below.)

The agar lanes were prepared by casting the agar mixture into a black-anodized aluminum frame or mold that defined four parallel channels (Figure 1). The frame rested on a glass coverslip that was coated with a thin, transparent silicone elastomer sealant (Sylgard 184, Dow Corning). The humidity of the agar was maintained by covering the lanes with a clear polycarbonate lid during measurements. GFP fluorescence excitation was provided by light from a blue light-emitting diode (LED) that was passed through an excitation filter (Thorlabs MF469-35) and diffusively scattered toward the sample by a light dome (Figure 1). The light dome was a plastic hemisphere (15 cm diameter) whose interior was coated with a high-reflectance, nonfluorescing $BaSO_4$ paint.[17] Multiple scattering of the excitation light within the dome yielded highly uniform illumination of the agar lanes: the variation in illumination across the image field was less than 3%. No excitation light was required for the bioluminescence measurements. Luminescence and the OD probe light (see below) from the four parallel lanes were collected through the same optical path (Figure 1) and imaged on a CCD camera.

The lane/coverslip assembly was seated on a black anodized aluminum baseplate containing an array of pinholes (0.7 mm diameter) that allowed in situ measurements of the agar OD: green LED light was directed upward through the pinholes (from beneath the baseplate) and through the agar to produce a transmitted light image on the camera. Using a timer circuit to switch between two light sources (blue GFP fluorescence excitation vs green pinhole light for OD) in alternate exposures, we collected a sequence of OD and fluorescence/bioluminescence images of each lane over the measurement period.

We introduced exogenous AHL into an agar lane by depositing a small volume (v = 1 μL) of AHL stock solution (c = 100 nM or 1 μM 3OC6-HSL in water) onto the surface of the agar at one terminus of the lane. The final (fully diffused, $t \to \infty$) AHL concentration C_∞ resulting from this initial loading is related to v, c, and the lane volume (=wdL) as $C_\infty = cv/wdL$. The figures below indicate the values of C_∞ used in each lane. We used small C_∞ (near 1 nM) to prevent the generation of a very rapidly saturating QS response throughout the lane. To generate the simple diffusion pattern in Figure 2, which verified the one-dimensional diffusion in the agar lanes, we added fluorescein dye (CAS no. 2321-07-5, Sigma Chemical) instead of AHL solution.

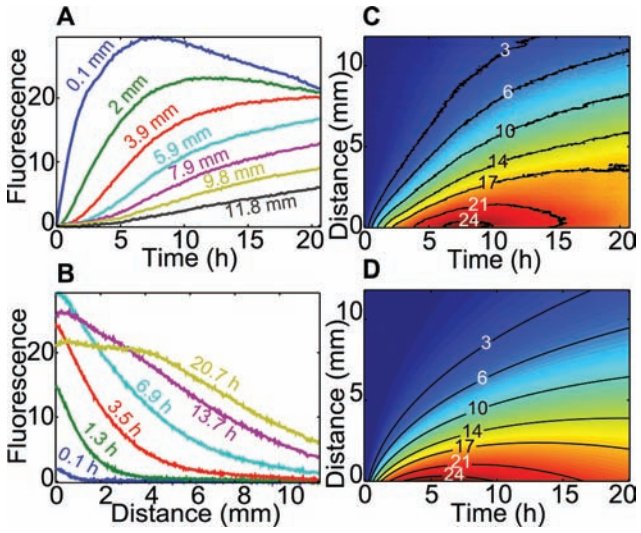

Figure 2. Diffusion of fluorescein dye along an agar lane. (A, B) The fluorescence is plotted as a function of (A) time t and (B) distance x from the dye droplet. (C) The contour lines in a map of fluorescence vs x and t show the $x^2 \sim 2Dt$ behavior that is characteristic of simple diffusive spreading. (D) Contour map generated by solving eq 2 by the finite difference method, based on $D = 1.5 \times 10^{-6}$ cm^2/s and using the same dye loading and boundary conditions as in (C). Contour labels indicate dye concentrations in μM.

Images were recorded on a CCD camera (1300 × 1030 array of 6.7 μm pixels with 12-bit readout, cooled to −10 °C, MicroMax, Princeton Instruments) through a 2× matched achromatic lens pair (MAP1075150-A, ThorLabs) and a GFP emission filter (MF525-39, Thorlabs). CCD images were collected with exposure times of ∼1−10s at a repetition rate of 0.004 Hz over periods of 20−24 h. The CCD images were hardware-binned by 5 pixels in the y direction (transverse to diffusion) and 2 pixels in the x direction (along the direction of diffusion). The image frame captured a 13.8 mm length along each of the four lanes, or nearly half of each 32 mm lane.

MATHEMATICAL MODEL

We constructed a mathematical model for the activation of the QS circuit in the sensor strain (*E. coli* + pJBA132) in response to diffusing AHL. The major features of the model are summarized briefly here. The SI provides a complete description of the model and its parametrization from multiwell-plate data.

Our multiwell-plate data suggested (as other modelers have noted[13,14]) that the formation of fluorescent GFP is best modeled as a multistage process, where the as-synthesized GFP is nonfluorescent but matures into the fluorescent form. We therefore modeled five variables: the cell concentration $n(x,t)$, the AHL concentration $C(x,t)$, and the concentration of each of three forms of the GFP protein.[13,14] These forms are the as-synthesized (e.g., unfolded) nonfluorescent protein U_1 [concentration denoted as $U_1(x,t)$], a folded nonfluorescent form U_2, and the mature fluorescent protein G. Although only G is observable in the experiments, we used the measurement units of counts per image pixel to represent the concentrations

dx.doi.org/10.1021/ja211593q | J. Am. Chem. Soc. 2012, 134, 5618−5626

of all three forms. AHL diffuses at a rate D (eq 2) and activates the synthesis of U_1 according to a nonlinear (Hill) function $f(C)$ (eq 3). U_1 and U_2 are converted to U_2 and G at rates m_1 and m_2, respectively. All three forms are degraded according to Michaelis–Menten kinetics.[13]

The equations and initial conditions of the model are summarized below:

$$\frac{dn}{dt} = n\alpha\left(1 - \frac{n}{K}\right) \tag{1}$$

$$\frac{\partial C}{\partial t} = D\frac{\partial^2 C}{\partial x^2} \tag{2}$$

$$\frac{\partial U_1}{\partial t} = \gamma f(C)\alpha n\left(1 - \frac{n}{K}\right) - m_1 U_1 - g(U_1) \tag{3}$$

$$\frac{\partial U_2}{\partial t} = m_1 U_1 - m_2 U_2 - g(U_2) \tag{4}$$

$$\frac{\partial G}{\partial t} = m_2 U_2 - g(G) \tag{5}$$

$$n(0) = n_0 \tag{6}$$

$$C(x, 0) = \begin{cases} C_\infty L/\nu & 0 \le x \le \nu \\ 0 & \nu < x \le L \end{cases} \tag{7}$$

$$U_1(x, 0) = U_2(x, 0) = G(x, 0) = 0 \tag{8}$$

$$\frac{\partial C}{\partial x}(0, t) = \frac{\partial C}{\partial x}(L, t) = 0 \quad \text{for } t > 0 \tag{9}$$

where

$$f(C) = \frac{C^m(x, t)}{a^m + C^m(x, t)} \tag{10}$$

and

$$g(V) = \frac{k_1 V}{k_2 + U_1 + U_2 + G} \tag{11}$$

and V may be U_1, U_2, or G. The parameters appearing in eqs 1–11 are defined in Table 1.

Table 1. Definitions of the Model Variables and Parameters (Values of the Parameters Are Given in the SI)

Variable/ Parameter	Definition
n	cell concentration
α	intrinsic cell growth rate (h^{-1})
K	cell-carrying capacity
C	AHL concentration (nM)
D	AHL diffusion constant (mm^2/h)
U_1	concentration of unfolded GFP (counts/pixel)
γ	proportionality factor (counts/pixel)
f	cooperative switch function
a	half-activation constant (nM)
m	Hill coefficient (dimensionless)
m_1	folding rate of GFP (h^{-1})
$g(V)$	rate of degradation of GFP in form V (counts $pixel^{-1}$ h^{-1})
k_1	maximum degradation rate (counts $pixel^{-1}$ h^{-1})
k_2	Michaelis constant (counts/pixel)
U_2	concentration of folded but nonfluorescent GFP (counts/pixel)
m_2	maturation rate of GFP (h^{-1})
G	concentration of fluorescent GFP (counts/pixel)
n_0	initial cell concentration
C_∞	fully diffused concentration of AHL (nM)
L	length of the agar lane (mm)
ν	length of the loading region (mm)

RESULTS

The LuxI/LuxR circuit at the core of bioluminescence regulation in the marine bacterium *V. fischeri* is an important model QS system with homologues in many other organisms.[2] LuxI is the synthase for 3OC6-HSL, which is an AHL that diffuses freely across the cell membrane and interacts with the cytoplasmic receptor LuxR to form a transcriptional activator for the *lux* operon, *luxICDABEG* (Figure 1). The *lux* operon encodes LuxI as well as the bacterial luciferase and other enzymes necessary for bioluminescence. However *lux* regulation in *V. fischeri* is also subject to other regulatory inputs that may complicate modeling. Therefore, we designed our mathematical model around a simpler, *E. coli*-based LuxI/LuxR system. We focused on an AHL-sensor strain of *E. coli* constructed by Andersen et al.[15] that harbors the plasmid pJBA132. This plasmid places expression of GFP(ASV), an unstable green fluorescent protein reporter, under the control of the *luxI* promoter.[15,18] However, it lacks the *luxI* gene that encodes the AHL synthase. Therefore, the sensor strain produces the LuxR receptor for the AHL, responds to exogenous AHL by producing GFP(ASV) (hereinafter GFP), and yet is unable to manufacture its own AHL. We also studied two strains of *V. fischeri*: The first is VCW267, a synthase-deficient mutant (in ES114 background) of the bacterium (Figure 1). It responds to exogenous 3OC6-HSL by producing weak bioluminescence but cannot manufacture 3OC6-HSL. The second is MJ11, a wild-type *V. fischeri* with intact AHL synthesis capability that is known for its brightness in culture.[19] In MJ11 activation of the *lux* operon by 3OC6-HSL triggers expression of the *luxI* gene for the AHL synthase (and hence positive feedback in AHL production) as well as the bioluminescence genes *luxCDABEG*.

For a spatially homogeneous system (i.e., where the right-hand side of eq 2 is equal to zero), the model given by eqs 1–9 describes the evolution of the mature, fluorescent GFP concentration $G(t)$ and the cell concentration $n(t)$ for a given AHL concentration C. The cell concentration $n(t)$ is presumed to be proportional to the experimentally measured optical density. We measured the fluorescence and OD of the sensor strain in a multiwell plate (containing well-mixed bacteria/AHL/medium) and fit the data to this space-independent model (see the SI). This fit yielded a set of parameters (Table 1) that describe the QS response in the sensor strain.

After parametrizing the model, we introduced a spatially heterogeneous AHL concentration $C(x,t)$ via eq 2. Then eqs 1–9 give a space- and time-dependent $G(x,t)$ and $\partial G/\partial t$ in response to the diffusing $C(x,t)$. Using a literature estimate for the 3OC6-HSL diffusion constant in water at room temperature ($D \approx 5.5 \times 10^{-6}$ cm^2/s[7,20]) and the parameters from our well-plate fit, we then simulated the response of the sensor strain, $G(x,t)$, to the concentration of the diffusing AHL in the agar lane, $C(x,t)$.

Diffusion of a Dye. The simplest spatiotemporal pattern we might expect to observe in the lanes is the familiar one-dimensional spreading pattern generated by Fick's Law (eq 2). Figure 2 verifies that this pattern is obtained when a soluble dye (rather than an autoinducer) is introduced into an agar lane.

dx.doi.org/10.1021/ja211593q | J. Am. Chem. Soc. 2012, 134, 5618–5626

We loaded 1 μL of a fluorescein solution (~0.2 μM in water) at one terminus ($x = 0$) of a lane containing an agar/*E. coli* mixture at $t = 0$ and allowed it to diffuse along the length of the lane. As measured by the fluorescence, the concentration $C(x,t)$ showed a strong mixing of time and space dependence, with rapid changes at short distances and early times giving way to slower spreading at longer distances and later times. The same patterns were observed regardless of whether bacteria were present in the agar lane. These patterns should be contrasted with the patterns induced by a diffusing AHL signal (see below).

Figure 2 also shows the precise solution[12] to the diffusion equation (eq 2) as obtained in a finite difference calculation based on our experimental configuration. The initial loading of the dye at the lane terminus was modeled as a step function in the initial concentration $C(x,t = 0)$, which subsequently spread according to eq 2. The curved contours on the dye concentration maps for both the experiment and the calculation reflect the signature $x^2 \sim 2Dt$ behavior of simple diffusive spreading. The close agreement of the experimental and theoretical $C(x,t)$ values verifies that our imaging method provides a quantitative measure of fluorophore concentration and confirms that diffusion through the lanes is essentially one-dimensional, as expected. Comparing the formal solution to the data allowed us to estimate $D \approx 1.5 \times 10^{-6}$ cm^2/s for the diffusion of fluorescein in 0.75% agar.

Sensor Strain and AHL Diffusion: Synchronized Kinetics. Figure 3 shows the pattern of GFP fluorescence of the sensor strain, $G(x,t)$, induced by a diffusing AHL signal (3OC6-HSL). Movie S1 in the SI shows these data as time-lapse images. The AHL signal readily activates GFP production at a substantial distance from the diffusing source, with nanomolar AHL loadings inducing a response that extends more than ~1 cm from the droplet located at $x = 0$. The figure also shows an interesting qualitative property of the bacterial response: $G(x,t)$ has a similar kinetic profile at different physical locations x, even though the magnitude of the response varies with x. That is, while GFP expression is weaker at greater distances x, the timing of that response is surprisingly insensitive to x. Similarly the x dependence of $G(x,t)$ is similar at different times t, with t affecting the overall magnitude more than the shape of G. In this regard, the spatial and temporal properties of the QS response have a simple, synchronized quality. This distinguishes them from the dye diffusion patterns (Figure 2), whose x and t dependence are closely entwined.

We observed the same behavior in the *lux*-regulated bioluminescence of the VCW267 (synthase-deficient) *V. fischeri*. As with the sensor strain, the QS circuit is activated nearly ~1 cm from the AHL source droplet (Figure 4). Furthermore the temporal pattern of activation shows only weak dependence on the distance x of diffusion. Even though the AHL signal diffuses according to $t \sim x^2$, the kinetics (although not the overall amplitude) of the *lux* responses at all locations within the range

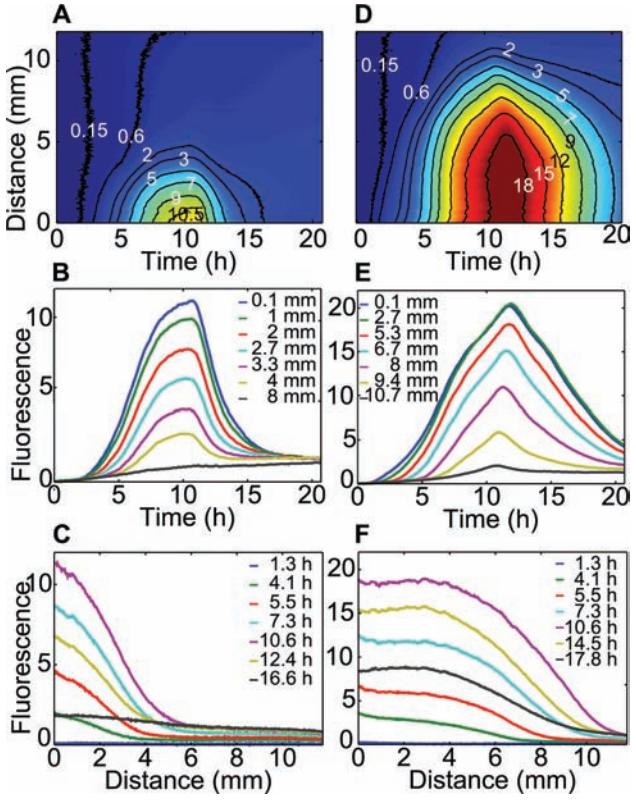

Figure 3. Response of the sensor strain (*E. coli* + pJBA132) to diffusing AHL. (A) and (D) show $G(x,t)$, the spatiotemporal pattern of reporter fluorescence, following deposition of an AHL (3OC6-HSL) droplet at the terminus ($x = 0$) of an agar lane at $t = 0$. The quantity of AHL introduced was sufficient to produce a final (fully diffused) concentration of $C_\infty = 0.4$ nM (A–C) or 4 nM (D–F) in the lane. (B) and (E) show slices through $G(x,t)$ at fixed distances x, while (C) and (F) show slices through $G(x,t)$ at fixed times t.

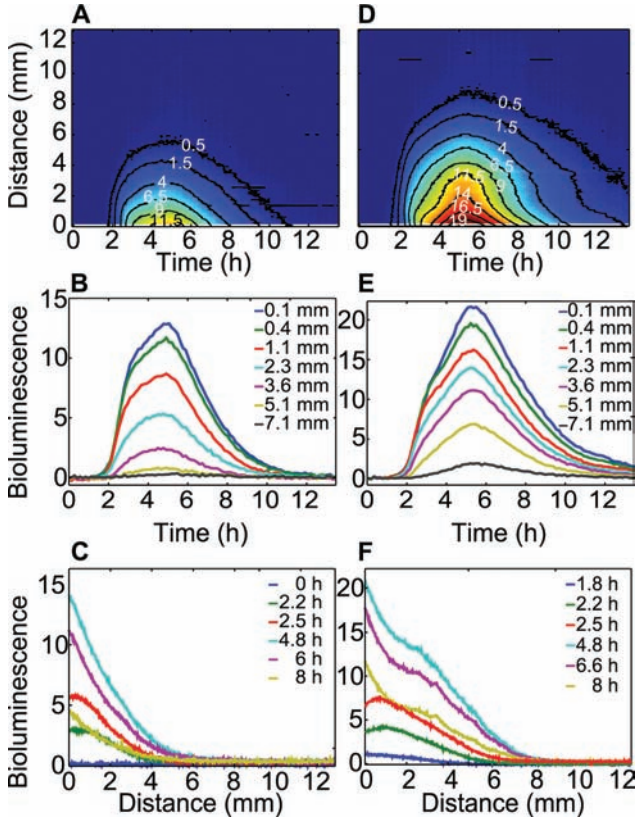

Figure 4. Bioluminescence response of *luxI*-deficient *V. fischeri* VCW267 to diffusing AHL. (A) and (D) show the bioluminescence as a function of x and t following deposition of a 3OC6-HSL droplet at the terminus ($x = 0$) of an agar lane at $t = 0$. The quantity of AHL introduced was equivalent to $C_\infty = 400$ nM (A–C) or 2 μM (D–F). (B) and (E) show slices through the bioluminescence pattern at fixed distances x, while (C) and (F) show slices at fixed times t.

dx.doi.org/10.1021/ja211593q | J. Am. Chem. Soc. 2012, 134, 5618–5626

$0.1 \leq x \leq 7$ mm are similar. Movie S2 in the SI shows these data as time-lapse images.

Simulations from the Model. We tested whether our mathematical model could predict the spatiotemporal patterns $G(x,t)$ that were observed for the *E. coli* sensor strain and *V. fischeri* VCW267. Figure 5 shows the $G(x,t)$ generated by the model for parameter values appropriate for the *E. coli* strain. The simulations agree qualitatively and quantitatively with the experimental data in Figure 3: For $C_\infty = 4$ nM AHL, the model predicts a pattern of activation extending to ~1 cm, with its response peaking near $t = 11-12$ h across that spatial range. The simulation for $C_\infty = 0.4$ nM AHL also matches the experimental result. As in the experimental data, $G(x,t)$ reaches its peak at nearly all locations x at nearly the same time t, even though the AHL concentration that induces that response (Figure 5 D) has a complex spatial and temporal profile. This comparison of the simulation and data indicates that the key ingredients of the model—simple diffusion of a signal that activates gene expression nonlinearly in a population that grows logistically—are sufficient to capture the long-range, synchronized character of the observed spatiotemporal patterns.

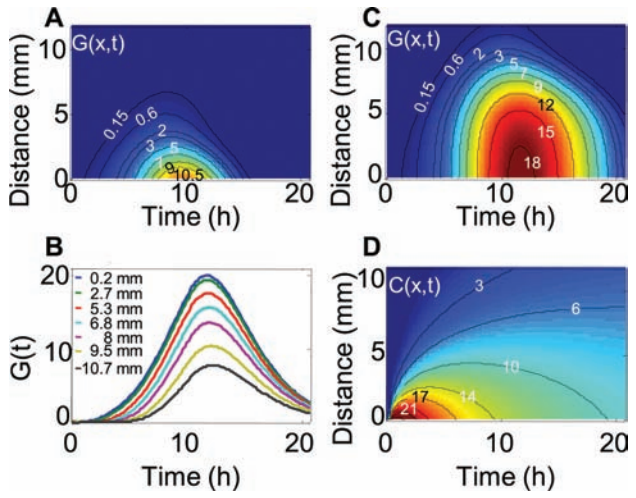

Figure 5. Patterns of expression predicted for the *E. coli* + pJBA132 sensor strain in response to diffusing AHL. The patterns were generated by simulation using the model (see Mathematical Model and the SI), assuming a final AHL concentration of $C_\infty = 0.4$ nM (A) or 4 nM (B, C). (D) shows the concentration of diffusing AHL, $C(x,t)$ (in μM), for $C_\infty = 4$ nM and a diffusion constant $D = 5.5 \times 10^{-6}$ cm^2/s.

Response of a Wild-Type QS Strain. To see how these patterns are affected by the presence of the AHL synthase, we studied the bioluminescence response of wild-type *V. fischeri* (strain MJ11) containing an intact *luxI* gene and therefore capable of positive feedback in AHL synthesis. In fact, this strain produces AHL (3OC6-HSL) so prodigiously that adding exogenous AHL at the lane terminus caused only a transient, local enhancement of the bioluminescence of the full lane: for small x and early t, the diffusing exogenous AHL ($C_\infty = 0$, 1, 6, or 60 nM) generated a spreading pattern similar to those in Figure 3 and Figure 4. However, by $t \approx 5$ h, the basal production of 3OC6-HSL had induced a bright bioluminescence at all x that overwhelmed the spreading pattern near the droplet (movie S3 in the SI).

However, the MJ11 system did display an intriguing phenomenon shortly after the midpoint of the growth curve, after the bioluminescence had reached its maximum. Figure 6 shows that a second burst of luminescence appeared at this time, originating as a localized brightness near the lane terminus and then traveling down the length of the lane. A time-lapse image (movie S3) shows this burst as a traveling pulse of bioluminescence moving through the lane at a speed of 0.1–0.3 mm/min at $t \approx 11$ h. This wavelike excitation appeared at the same growth stage in all four agar lanes, regardless of the AHL loading. [Full-lane images (not shown) suggest that similar bioluminescence bursts may originate simultaneously at both lane termini ($x = 0$, L) and meet at the lane center.] Although a traveling pulse that was not induced by exogenous AHL was unexpected, it indicates that *lux* regulatory mechanism of the wild-type organism has the capability to generate and sustain excitations that can propagate over macroscopic distances.

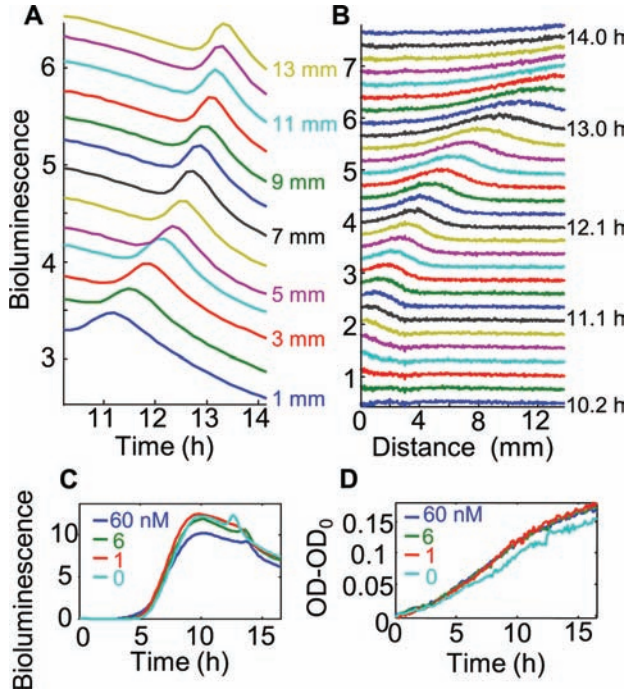

Figure 6. Traveling excitation of the bioluminescence in wild-type *V. fischeri*. In an agar lane containing the MJ11 strain, an excess bioluminescence was observed to originate at the lane terminus ($x = 0$) at $t \approx 11$ h and then propagate through the lane (also see movie S3 in the SI). The figure shows slices through the bioluminescence data as functions of (A) time t and (B) distance x from the lane terminus. The data are vertically offset for clarity, and the bioluminescence is shown in arbitrary units. In this experiment, a droplet of exogenous AHL equivalent to $C_\infty = 1$ nM was introduced at $x = t = 0$, although the pulse also occurred in the absence of exogenous AHL. (C) The total bioluminescence of each lane (integrated over x) peaks at $t \approx 10$ h, shortly before the onset of the traveling pulse, which is visible here as a brief spike in the bioluminescence at $t \approx 12-14$ h. Labels indicate exogenous AHL loadings (C_∞). (D) The optical density of the agar [measured relative to OD($t = 0$)] indicates that the bacteria attain their maximal growth rate near $t = 10$ h, shortly before the appearance of the excitation.

DISCUSSION

The defining characteristic of QS gene regulation is the production and detection of a diffusible cell-to-cell signal. It is thus somewhat surprising that QS is often studied under

dx.doi.org/10.1021/ja211593q | J. Am. Chem. Soc. 2012, 134, 5618–5626

laboratory conditions that minimize the role of diffusion. In well-stirred, physically homogeneous cultures, the concentration of autoinducer is spatially uniform and (setting aside stochasticity in expression) the regulatory response across the sample is well-synchronized. However, many of the natural environments colonized by QS bacteria are spatially extended and physically and chemically heterogeneous. Here the diffusional properties of the autoinducers should be expected to play an important role in limiting the range and kinetics of cell-to-cell signaling.[7] In many cases, the efficiency of diffusion is itself an important environmental parameter that QS mechanisms may be ideally suited to probe.[4,5] Our goals in this work were to analyze the interplay between signal diffusion and QS response, to model the spatial and temporal response mathematically, and thereby to understand quantitatively how QS regulation synchronizes gene regulation on macroscopic length scales in the absence of advective mixing.

One would not expect a signal diffusing at $D \approx 5.5 \times 10^{-6}$ cm^2/s to elicit a coordinated regulatory response from a bacterial population that is dispersed over millimeters or centimeters. However, in our experiments the QS signal produced a well-synchronized response in a spatially extended population. For both the pJBA132 sensor *E. coli* (Figure 3) and the VCW267 *V. fischeri* (Figure 4), the diffusion of AHL through agar induced a robust *lux* response at macroscopic distances of ~1 cm. This is consistent with a recent study in which AHLs diffusing from a *P. aeruginosa* biofilm activated a QS reporter strain located up to 8 mm away.[9] We expect that even greater distances could be achieved in our experiment if larger AHL loadings were used.

The practical limit to the physical range of QS signaling is most likely fixed by the solubility and stability of the signal molecule in the natural environment. For the AHL signals used by many Gram-negative species, the solubility is limited by the hydrophobic acyl side chain, which can range from four to 18 carbons in length. The longer-chain AHLs have poor solubility and would presumably be much less mobile in aqueous environments. They may tend to partition out of the fluid phase. The signaling range would also be reduced by environmental degradation of the autoinducers. AHLs may be actively degraded by acylases, lactonases, and oxidoreductases that are produced by other bacteria in the environment.[21] AHL autoinducers are also vulnerable to chemical hydrolysis of the lactone ring, a reaction that is accelerated greatly under alkaline conditions: While our studies were conducted near pH 7, where AHL has a half-life of many hours, the half-life above pH 8 is measured in minutes.[20] For a diffusion constant $D \approx 5.5 \times 10^{-6}$ cm^2/s, the physical range of signaling under those conditions likely would not exceed ~1 mm.

A number of previous authors have constructed mathematical models to describe the dynamics of QS systems, especially LuxI/LuxR. These include studies of stability and bistability in the response to AHL,[22,23] noise in QS,[24] fluctuations,[25] signal crosstalk,[26] and QS control of GFP reporter production.[14] Most such treatments have set aside any interplay between the spatial diffusion of AHL and the QS dynamics by assuming a homogeneous or well-stirred chemical environment. However, spatial and temporal heterogeneity in the production and accumulation of AHL must play a role in structured microbial communities.[7] Even in the spatially homogeneous model of Garde et al.,[14] it was apparent that the transcriptional response to a C4-HSL autoinducer was so slow that the molecule likely diffuses at least 1 mm before binding to its receptor. Hence, the AHL does not truly act "locally", and spatial diffusion is a physically essential component of QS.

We constructed a spatial and temporal model (eqs 1−9 in Mathematical Model) and compared it with our experimental findings on the *E. coli* + pJBA132 sensor strain. The model considers simple diffusive transport of AHL and its interaction with logistic growth of the bacterial population and nonlinear (Hill-function) transcriptional activation in the QS circuit. It also includes a Michaelis−Menten process for degradation of the unstable GFP.[13] Simulations obtained using the model (Figure 5) capture the key features of the experimental data in Figure 3.

One of those features is the synchronized kinetics of the QS response. If AHL diffuses away from a point source, eq 2 requires that the concentration of AHL exhibit a nonlinear dependence on both x and t: the time t required to reach a given AHL concentration scales roughly as the square of the distance x from the source, suggesting that bacterial cells located at greater x will become activated at significantly later t. However, for both the pJBA132 sensor *E. coli* (Figure 3) and the VCW267 *V. fischeri* (Figure 4), the time course of the response to AHL was relatively insensitive to x. The simulations show the same property (Figure 5). Although the overall amplitude of the QS response is weaker when the AHL has diffused a greater distance, the time t at peak response is not sensitive to the distance that the AHL has diffused.

We can quantify this spatial synchrony by performing a singular-value decomposition[27] of the $G(x,t)$ data:

$$G(x, t) = u_1(x)sv_1(t) + u_2(x)sv_2(t) + u_3(x)sv_3(t) + \ldots \quad (12)$$

Here the $u_i(x)$ and $sv_i(t)$ are basis vectors that reconstruct the data, such that the magnitude of each component $u_i(x)sv_i(t)$ decreases as i increases from $i = 1$ to i_{max} (the limit i_{max} is equal to the number of measured x or t values, whichever is smaller.) Applying this analysis to the sensor strain data in Figure 3, we find that the first term $u_1(x)sv_1(t)$ alone captures roughly 90% of the data set $G(x,t)$, leaving only a small residual (Figure 7). The first and second terms ($i = 1, 2$) together describe more than 94% of $G(x,t)$. The subsequent terms ($i > 2$) are primarily measurement noise.

Therefore, to an excellent approximation, we can view the spatiotemporal pattern $G(x,t)$ as the product of two independent functions: $G(x,t) \approx u_1(x)sv_1(t)$, where $u_1(x)$ contains all of the spatial dependence of the QS response and $sv_1(t)$ contains all the time dependence. $u_1(x)$ has a cosine shape; it is virtually flat for $x < 5$ mm and approaches zero only for $x > 10$ mm (Figure 7). The temporal component $sv_1(t)$ has just one sharp peak at $t \approx 11$ h. The fact that the data can be described so simply is very uncharacteristic of a diffusion-controlled process: the functions $C(x,t)$ that solve the diffusion equation (eq 2) for the relevant Neumann or no-flux boundary conditions at $x = 0, L$ are not usually dominated so strongly by a single pair of basis vectors.

Figure 7 shows that both the experiments and simulations exhibit the same separability in x and t, yielding very similar components $u_1(x)$ and $sv_1(t)$. This demonstrates that no active transport of AHL is required in order to explain the coordinated QS response that we observe: The combination of a temporally peaked (logistic) bacterial growth characteristic and a cooperative response to the AHL concentration evidently permit a well-synchronized burst of QS activation as the AHL diffuses through the environment.

Turning then to wild-type *V. fischeri* (MJ11 strain, +*luxI*), we observed an intriguing phenomenon. As shown in Figure 6 and

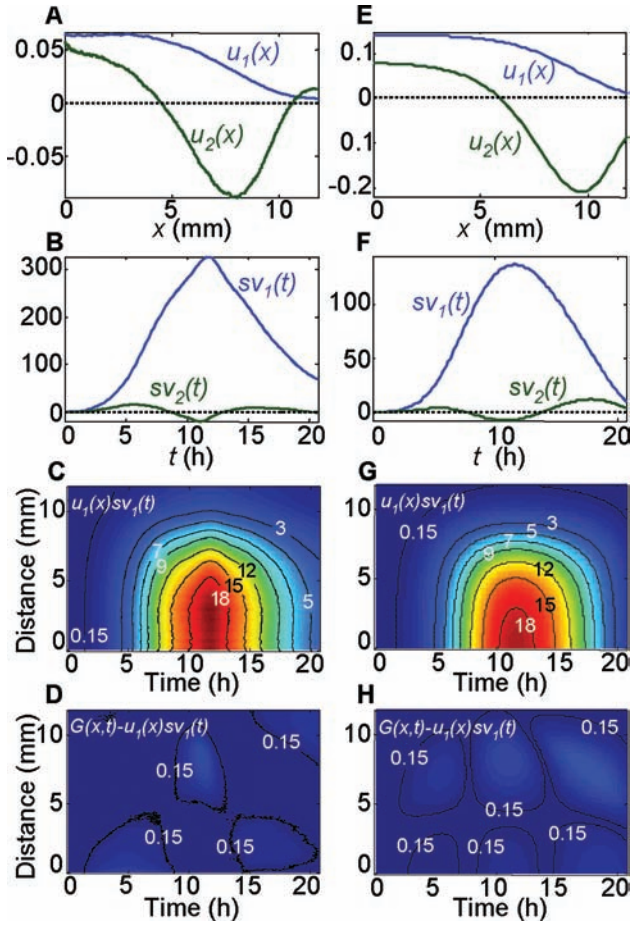

Figure 7. Mathematical decomposition of the spatiotemporal pattern. According to the decomposition in eq 12, the $G(x,t)$ data for the *E. coli* + pJBA132 sensor strain can be described as the product of a spatial function $u_1(x)$ and a temporal function $sv_1(t)$: $G(x,t) \approx u_1(x)sv_1(t)$. (A) Leading components $u_1(x)$ and $u_2(x)$ in eq 12. (B) Leading components $sv_1(t)$ and $sv_2(t)$. (C) The product $u_1(x)sv_1(t)$, which can be compared to the full set of original $G(x,t)$ data shown in Figure 3D. (D) The residual $G(x,t) - u_1(x)sv_1(t)$, here shown on the same color scale as in (C). (E, F) Leading components in the decomposition of the simulated $G(x,t)$ obtained from our model. (G) The product $u_1(x)sv_1(t)$ for the simulated $G(x,t)$. (H) The residual $G(x,t) - u_1(x)sv_1(t)$ calculated for the simulation.

movie S3 in the SI, a pulse of bioluminescence appeared at one terminus of the agar lane at $t \approx 11$ and then traveled the length of the lane. This pulse, with a well-defined width of 2−4 mm and a speed of 0.1−0.3 mm/min, more closely resembled a propagating wave than diffusive spreading. Spatially propagating excitations have been observed in some synthetic, designed QS systems.[11] However, we are not aware of any other observations of traveling excitations in wild-type QS systems.

We have not determined the mechanism of the excitation. Propagating waves of gene activation are probably possible within systems of the LuxI/LuxR type.[28] However, we do not believe that the observed phenomenon arises within the LuxI/LuxR circuit alone, as the pulse appeared shortly after the midpoint of the bacterial growth curve, at which time the basal production of quorum signals (including 3OC6-HSL) had led to autoinduction at all x, the culture had already achieved maximum bioluminescence output, and the growth rate had begun to slow. Hence, the appearance of the pulse was insensitive to any initial loading of AHL (3OC6-HSL) at the lane terminus and initiated at the lane terminus whether or not exogenous AHL was present. This suggests that it is triggered by local heterogeneities in population density or nutrient conditions that are amplified by proximity to the boundary wall.

Bioluminescence regulation in *V. fischeri* is much more complex than the LuxI/LuxR mechanism alone. First, the *lux* genes of *V. fischeri* receive input from three QS signals: 3OC6-HSL, *N*-octanoyl-L-homoserine lactone (C8-HSL), and a furanosyl borate diester designated AI-2. The C8-HSL and AI-2 signals are received and combined through a phosphorelay that controls *litR*, which in turn regulates expression of *luxR* and a number of other genes.[29,30] Second, as in most QS systems, *lux* also interacts with or responds to a number of other physiological mechanisms and environmental factors.[30] The availability of oxygen is one example. Bioluminescence of *V. fischeri* is repressed by the ArcAB system, and this repression is alleviated in the presence of oxygen or oxidative stress.[31] Bioluminescence is also subject to catabolite repression, in which the presence of carbohydrates such as glucose inhibits the expression of certain other enzymes. In *V. fischeri*, the presence of CRP/cAMP, which signals the absence of glucose, interacts with *lux* by activating transcription of LuxR, the cytoplasmic receptor for the 3OC6-HSL autoinducer. Therefore, while the presence of glucose inhibits the QS response, that response may be enhanced as nutrient availability and growth rate begin to decline.[32]

Therefore, one may speculate that the observed wave of bioluminescence results when a transient condition during growth interacts with *lux* regulation to create a behavior that is spatially and temporally unstable. For example, as the carbohydrate in the medium becomes depleted and catabolite repression of the *lux* genes is alleviated, a brief burst in bioluminescence could appear, which would further deplete the medium in adjacent regions. This could trigger a wave of derepression moving at a speed that is dependent on the speed of the transcriptional mechanisms as well as the concentrations and diffusion constant of the remaining carbohydrate. Designing reporter strains to test such mechanisms and constructing an appropriate quantitative model for the traveling excitation would be an interesting future direction.

■ CONCLUSION

Diffusion of an AHL signal can activate quorum-regulated gene expression over macroscopic distances, generating spatial and temporal patterns that differ significantly from the patterns of simple diffusion. These patterns show suprising synchrony on length scales of at least ∼1 cm and time scales of ∼10 h. Therefore, while we would not have expected that a signal diffusing at typical small-molecule rates could synchronize expression in a population on these length and time scales, the interaction of signal diffusion with nonlinear bacterial growth and cooperative transcriptional activation narrows the time window of the regulatory response. We expect that this could be significant in certain biological contexts. For example, a small subpopulation of cells within a larger population could respond to a local environmental condition by releasing a diffusible signal that would elicit a synchronized population-wide response. Such a "master−slave" dynamic would be a departure from the more conventional "democratic" scenario of QS as population-counting. The traveling excitation that we observed in the bioluminescence of the wild-type *V. fischeri* strain is an even more dramatic dynamic that is even less characteristic of diffusion. The mechanism of this excitation will be a subject of future study.

dx.doi.org/10.1021/ja211593q | *J. Am. Chem. Soc.* 2012, 134, 5618−5626

Our findings also raise questions of whether the timing of a population-wide response could be manipulated through the use of combinations of different chemical signals. Many QS networks synthesize and detect multiple chemical species (e.g., AHLs with various chain lengths) that differ in mobility, solubility, and cell permeability. These may allow additional dimensions of control over the shape or timing of a population-wide response. As more researchers explore the ecological, environmental, and interspecies complexities of QS, we anticipate that the role of physical diffusion and its consequences for bacterial gene regulation will be more widely recognized.

■ ASSOCIATED CONTENT

Supporting Information

Greater detail on the mathematical model and the fits to the wellplate data, which provided the values of the parameters in Table 1 and the simulation of Figure 5; movies S1–S3 (QT) showing time-lapse images of AHL diffusion experiments conducted with the *E. coli* sensor strain, *V. fischeri* strain VCW267, and *V. fischeri* strain MJ11, respectively. This material is available free of charge via the Internet at http://pubs.acs.org.

■ AUTHOR INFORMATION

Corresponding Author

sjhagen@ufl.edu

Notes

The authors declare no competing financial interest.

■ ACKNOWLEDGMENTS

J.B.L. gratefully acknowledges funding support from the National Science Foundation under IGERT Award DGE-0801544. P.D.L. thanks Vlaams Academisch Centrum for hosting him as a research fellow during a sabbatical leave from the University of Florida. P.D.L. also gratefully acknowledges support received from the University of Florida through a Faculty Enhancement Opportunity, and the Universite Catholique de Louvain-la-Neuve for providing him with a visiting professorship in the fall of 2011.

■ REFERENCES

(1) Ng, W.-L.; Bassler, B. L. *Annu. Rev. Genet.* **2009**, *43*, 197–222.
(2) Waters, C. M.; Bassler, B. L. *Annu. Rev. Cell Dev. Biol.* **2005**, *21*, 319–346.
(3) Venturi, V.; Subramoni, S. *HFSP J.* **2009**, *3*, 105–116.
(4) Redfield, R. J. *Trends Microbiol.* **2002**, *10*, 365–370.
(5) Hense, B. A.; Kuttler, C.; Müller, J.; Rothballer, M.; Hartmann, A.; Kreft, J.-U. *Nat. Rev. Microbiol.* **2007**, *5*, 230–239.
(6) Dunn, A. K.; Stabb, E. V. *Anal. Bioanal. Chem.* **2007**, *387*, 391–398.
(7) Stewart, P. *J. Bacteriol.* **2003**, *185*, 1485–1491.
(8) Gantner, S.; Schmid, M.; Dürr, C.; Schuhegger, R.; Steidle, A.; Hutzler, P.; Langebartels, C.; Eberl, L.; Hartmann, A.; Dazzo, F. B. *FEMS Microbiol. Ecol.* **2006**, *56*, 188–194.
(9) Flickinger, S. T.; Copeland, M. F.; Downes, E. M.; Braasch, A. T.; Tuson, H. H.; Eun, Y.-J.; Weibel, D. B. *J. Am. Chem. Soc.* **2011**, *133*, 5966–5975.
(10) Whitaker, R. D.; Pember, S.; Wallace, B. C.; Brodley, C. E.; Walt, D. R. *J. Biol. Chem.* **2011**, *286*, 21623–21632.
(11) Danino, T.; Mondragon-Palomino, O.; Tsimring, L.; Hasty, J. *Nature* **2010**, *463*, 326–330.
(12) Crank, J. *The Mathematics of Diffusion*, 2nd ed.; Clarendon Press: Oxford, U.K., 1979.
(13) Leveau, J. H. J.; Lindow, S. E. *J. Bacteriol.* **2001**, *183*, 6752–6762.
(14) Garde, C.; Bjarnsholt, T.; Givskov, M.; Jakobsen, T. H.; Hentzer, M.; Claussen, A.; Sneppen, K.; Ferkinghoff-Borg, J.; Sams, T. *J. Mol. Biol.* **2010**, *396*, 849–857.
(15) Andersen, J. B.; Heydorn, A.; Hentzer, M.; Eberl, L.; Geisenberger, O.; Christensen, B. B.; Molin, S.; Givskov, M. *Appl. Environ. Microbiol.* **2001**, *67*, 575–585.
(16) Arsene, F.; Tomoyasu, T.; Bukau, B. *Int. J. Food Microbiol.* **2000**, *55*, 3–9.
(17) Takahashi, T.; Ikezawa, Y. White Standard Paint. U.S. Patent 6,555,608, 2003.
(18) Andersen, J. B.; Sternberg, C.; Poulsen, L. K.; Bjorn, S. P.; Givskov, M.; Molin, S. *Appl. Environ. Microbiol.* **1998**, *64*, 2240–2246.
(19) Mandel, M. J.; Wollenberg, M. S.; Stabb, E. V.; Visick, K. L.; Ruby, E. G. *Nature* **2009**, *458*, 215–218.
(20) Horswill, A. R.; Stoodley, P.; Stewart, P. S.; Parsek, M. R. *Anal. Bioanal. Chem.* **2007**, *387*, 371–380.
(21) Decho, A. W.; Frey, R. L.; Ferry, J. L. *Chem. Rev.* **2011**, *111*, 86–99.
(22) James, S.; Nilsson, P.; James, G.; Kjelleberg, S.; Fagerström, T. *J. Mol. Biol.* **2000**, *296*, 1127–1137.
(23) Williams, J. W.; Cui, X.; Levchenko, A.; Stevens, A. M. *Mol. Syst. Biol.* **2008**, *4*, 234.
(24) Cox, C. D.; Peterson, G. D.; Allen, M. S.; Lancaster, J. M.; McCollum, J. M.; Austin, D.; Yan, L.; Sayler, G. S.; Simpson, M. L. *OMICS* **2003**, *7*, 317–334.
(25) Zhou, T.; Chen, L.; Aihara, K. *Phys. Rev. Lett.* **2005**, *95*, No. 178103.
(26) Kuttler, C.; Hense, B. A. *J. Theor. Biol.* **2008**, *251*, 167–180.
(27) Press, W. *Numerical Recipes: The Art of Scientific Computing*, 3rd ed.; Cambridge University Press: Cambride, U.K., 2007.
(28) Jin, Y.; Zhao, X. *J. Biol. Dyn.* **2008**, *2*, 196–207.
(29) Visick, K. L. *J. Bacteriol.* **2005**, *187*, 3603–3606.
(30) Frederix, M.; Downie, J. A. *Adv. Microb. Physiol.* **2011**, *58*, 23–80.
(31) Bose, J. L.; Kim, U.; Bartkowski, W.; Gunsalus, R. P.; Overley, A. M.; Lyell, N. L.; Visick, K. L.; Stabb, E. V. *Mol. Microbiol.* **2007**, *65*, 538–553.
(32) Dunlap, P. V. *J. Mol. Microbiol. Biotechnol.* **1999**, *1*, 5–12.